Journal of
Microelectromechanical Systems

MEMS Tunable Photonic Crystal-Cantilever Cavity

Qiugu Wang, Depeng Mao, and Liang Dong

***Abstract*— We present an easy-to-implement microelectromecha-nical system-based tunable photonic crystal (PC) resonant cavity. This cavity is formed by embedding the tip of an electrostatically bendable cantilever into the center of a PC nanobeam structure. Owing to the presence of the cantilever, band edge resonant modes occur within the cavity that allow light transmission through a photonic barrier. When a voltage is applied, the cantilever deflection perturbs the optical fields of the band edge modes; this results in the modulation of both resonant wavelength and quality factor of the modes. The resonant wavelength of the cavity redshifts 13.5 nm when 97 volts is applied.**

***Index Terms*— Cantilever; electrostatic; cavity; photonic crystal**

I. Introduction

OPTICAL resonant cavities in photonic crystals (PCs) provide high quality factor (Q-factor) and small mode volume, and can be used to modify the interactions between light and matter. The capability to tune the optical properties of the PC cavities is essential to increase the adaptability of the PC-based resonators to different optoelectronic applications. Active media are often incorporated into the PC structures to tune the PC resonances. For example, the infiltration of liquid crystals into the PC cavities has enabled both the electrical and the thermal modulations of the effective refractive indices of the cavities [1], [2]. Many nonlinear electro-optical modulation approaches have been studied to tune PCs, using lithium niobate [3], [4], vanadium dioxide [5], optical carrier injection [6], and gradient optical force [7], [8]. In addition, fast light modulations at several gigahertz with low power consumption have been demonstrated, using a reverse-biased two-terminal p–n junction [9] and a three-terminal metal–oxide–semiconductor field-effect transistor-like diode [10]. This makes it possible to realize all-silicon-based monolithically integrated optoelectronic systems.

Microelectromechanical systems (MEMS) approach has been used to tune the optical properties of metamaterials by embedding nanocantilevers inside split-ring resonators (SRRs) [11] and complimentary SRRs [12]. By moving a dielectric plate towards a PC line-defect waveguide [13], or changing the height difference between a flexible PC waveguide and silicon rods [14], the optical transmittance of the waveguide can be tuned. Also, an array of plugs has been proposed to modulate the transmission of light through a PC structure [15]. In addition, our theoretical study [16] indicates a strong influence of the mechanical movement of a cantilever on the defect-mode field inside a PC. Despite these efforts, most MEMS-based tunable PCs require sophisticated structures, fabrications, and actuation methods.

In this paper, we demonstrate a novel MEMS-based tunable PC cavity that involves directly embedding the tip of a cantilever into a PC nanobeam-based waveguide structure, which we name as a PC-Cantilever Cavity (PC^3). The device is depicted in Fig. 1(a), where a nanobeam and a cantilever are integrated into the same Si device layer of a Si-on-insulator (SOI) wafer. The top thin Si device layer serves as an electrode while the thick handling Si layer of the SOI substrate acts as a ground for the device. This allows forming the PC^3 in the top Si layer using e-beam lithography, reactive ion etching, and wet etching-based release techniques. When a voltage is applied between the top and the bottom Si layers, the generated electrostatic force will bend the cantilever and thus perturb the optical field in the resonant cavity.

II. Design and Fabrication

Essentially, the PC^3 design is a modified version of a nanobeam cavity [17], [18]. The PC as shown in Fig. 1(a) has a triangular lattice with a periodicity of $P = 500$ nm and a hole size of $D = 400$ nm. In the nanobeam, a linear array of air holes is designed on each side of a central defect. The periodicity of the linear air holes is fixed at $p = 300$ nm, while the radii of the air holes gradually decrease from the center outwards along the horizontal direction. The air hole nearest to the central defect has the maximum radius $d_o = 125$ nm, while the air hole connecting to the feeding waveguide has the minimum radius $d_{10} = 88$ nm. To form a tunable cavity on the optical passage of the nanobeam, we removed several air holes from the PC lattice and filled the vacant region with the tip of a sword-like cantilever. The width and length of the cavity are $W_1 = 200$ nm and L $= 2.8$ μm, respectively. The width of the vacant region in the PC for housing the cantilever is $W_2 = 420$ nm.

Fig. 1(b) shows the scanning electron microscopic (SEM) images of the PC^3. The fabrication process flow for this device is briefly described in Fig. 1(c). Basically, the fabrication started with an SOI wafer with a 450-nm-thick top Si device layer and a 1-μm-thick buried oxide layer as a sacrificial layer. The top Si layer was doped with phosphorous of 2.5×10^{20} cm^{-3}, partially oxidized, and then etched to obtain a 200-nm-thick Si layer by a wet chemical etching method. Subsequently, the patterns of the PC^3 were formed in a resist layer of poly(methylmethacrylate) or PMMA using e-beam lithography, and then transferred to the top Si layer by deep reactive ion etching. Next, wet etching was used to release the cantilever by partially removing the buried oxide, while the two tapered feeding waveguides and the root part of the sword-shape structure (Fig. 1(b)), which supports the cantilever, still

Manuscript received ∗∗∗∗; revised ∗∗∗∗∗; accepted ∗∗∗∗∗. This work was supported by the U.S. National Science Foundation under Grant ECCS-0954765 and Grant ECCS-1711839. (*Corresponding author: Liang Dong*)

The authors are with Department of Electrical and Computer Engineering, Iowa State University, Ames, Iowa 50011, USA (ldong@iastate.edu).

D. Mao and Q. Wang contributed equally to this work.

Digital Object Identifier: 10.1109/JMEMS.2019.2936450

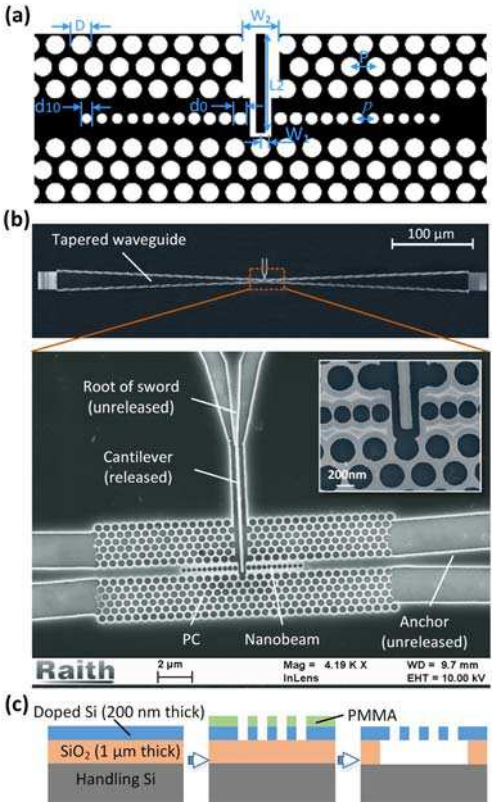

Fig. 1. (a) Schematic of the proposed PC^3 with the tip of a cantilever directly inserted into a PC-based nanobeam. (b) SEM photographs of the PC^3. The inset gives a closed-up view of the tip of the cantilever. (c) Schematic of the key fabrication processes for manufacturing the PC^3.

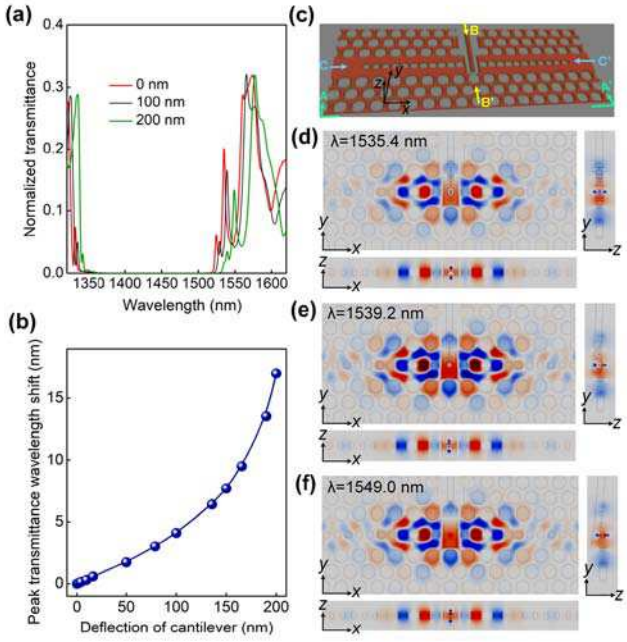

Fig. 2. (a) Normalized transmittance at different deflections of the cantilever: $\Delta z = 0$, 100 and 200 nm. (b) Resonant wavelength shift versus bending of the cantilever. (c) 3D schematic of the nanobeam-based PC^3. (d)–(f) Electric field (amplitude) distributions at the resonance mode of the nanobeam-based PC^3 with the deflection of $\Delta z = 0$ nm (d), 100 nm (e), and 200 nm (f). Each figure contains three parts showing the field distributions in the plane of X-Y, Y-Z, and X-Z across the lines A-A', B-B', and C-C', respectively.

remained anchored to the substrate. Thus, the proposed device was realized.

To characterize the device, an incident beam from a 1550 nm wavelength tunable laser was coupled to the device through an input grating coupler, and the output light was collected by a multimode fiber aligned to an output grating coupler on the other side of the device. An optical spectrum analyzer with a wavelength range of 1520 nm to 1620 nm was used to detect the transmission spectrum of the output light. To bend the cantilever, a D.C. voltage was applied between the top Si device layer and the back of the SOI substrate. All alignments were achieved under a microscope with the help of a motorized stage.

III. Results and Discussion

To understand how the mechanical bending of the embedded tip of the cantilever can influence the transmission spectrum of the PC^3, we first performed electromechanical simulations using the finite element analysis software COMSOL Multiphysics. This provided us with the mechanical deflections of the cantilever under different applied voltages. The obtained deflections were then used in the physical model of the cantilever for optical simulations. The optical simulations used an open-source freeware package MEEP, where the computed region covered the 200-nm-thick Si device layer and two 300-nm-thick sandwiching air layers in the thickness direction of the PC slab. The thick handling layer of the SOI substrate was excluded from the computation because the modal profiles in the PC^3 could hardly reach the handling substrate. All the boundaries of the computing region were applied with 150-nm-thick perfectly matched layers, and 20 periods of the photonic lattice in the $\Gamma - M$ direction were calculated. Fig. 2(a) shows the normalized transmittance under different displacements of the cantilever (Δz). The valley with zero transmittance between 1350 nm and 1520 nm corresponds to the photonic bandgap of the nanobeam. Fig. 2(b) summarizes the relationship between the wavelength shift of the transmission peak and the bending of the cantilever. A theoretical maximum shift of 17 nm is obtained when the cantilever completely bends out of the slab. The impact of the cantilever's deflection on the band edge resonant mode exhibits a nonlinear behavior, possibly because the optical field evanescently decays from the PC surface. As the cantilever deflects along the decay length of the field, its impact on the resonance becomes significant.

The origins of the resonance peaks can be understood from Fig. 2(d)–(f), which show the modal profiles of the PC^3 under different bending conditions. For example, in Fig. 2(d), at resonance, the highest field intensity in the PC^3 locates in the defect region occupied by the cantilever. The electric field is confined well within the cavity region in all the three dimensions, because the planar PC structure helps confine the in-plane field while in the out-of-plane direction the cantilever is thin enough to allow the transmission of light along the cantilever.

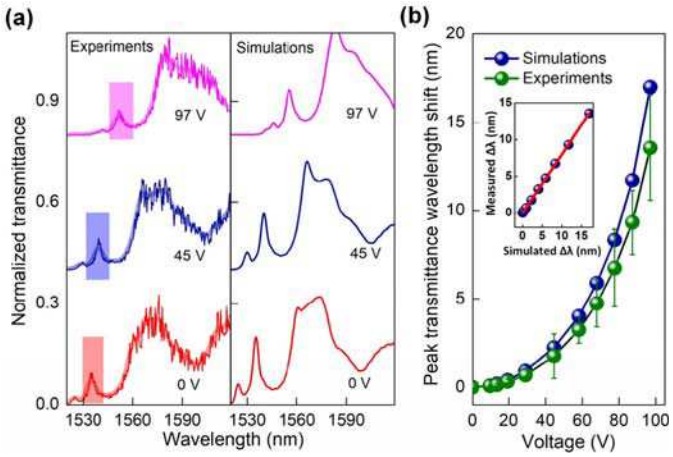

Fig. 3. (a) Measured (right panel) and simulated (left panel) normalized transmittance of the PC^3 under 0 V, 45 V, and 97 V. (b) Measured and simulated resonant wavelength shifts under different applied voltages. The inset gives the measured versus simulated results of the resonant wavelength shifts $\Delta\lambda$.

TABLE I

PERFORMANCE COMPARISONS FOR MEMS-BASED OUT-OF-PLANE TUNABLE PC CAVITIES IN THE NEAR-INFRARED WAVELENGTH RANGE

PC cavity structure	Maximum Q-factor	Maximum wavelength shift	Applied voltage range
Double-coupled PC cavity [19]	~72,000	~0.0635 nm	0–12 V
Split-beam PC cavity [20]	~67,500	~0.1167 nm	0–40 V
This work	~371	~13.5 nm	0–97 V

Fig. 3(a)–(b) show the measured transmittance of the PC^3 under different applied voltages. As the voltage increases from 0 to 97 V, the peak resonant wavelength is found to redshift from 1534 to 1547.5 nm, while the corresponding Q-factor reduces from 371 to 218. There is a good linearity between the measured and simulated wavelength shift, and the minor wavelength difference may be due to possible fabrication errors and inaccuracy of the model used in the optical simulation.

Table 1 compares the maximum Q-factor, maximum resonance wavelength shift, and applied voltage among several MEMS-based out-of-plane tunable PC cavities operating in the near-infrared wavelength range. The result shows that although the Q-factor of our device is relatively low, the device exhibits a considerable large resonance wavelength shift, possibly owing to the direct insertion of the cantilever's tip into the small breaking gap in the center of the nanobeam structure.

IV. CONCLUSION

In this work, we have demonstrated a MEMS-based tunable PC^3 device that involves inserting the tip of a cantilever into a nanobeam structure. The planar integration approach simplifies the fabrication process. The PC^3 design increases the tunability of the PC resonance. The results show that at 97 V, a maximum resonant wavelength shift of 13.5 nm was obtained for the PC^3 device.

REFERENCES

[1] S. Weiss, H. Ouyang, J. Zhang, and P. Fauchet, Electrical and thermal modulation of silicon photonic bandgap microcavities containing liquid crystals, *Opt. Express*, vol. 13, no. 1090, pp. 1090−1097, 2005.

[2] H. Xing, J. Li, Y. Shi, J. Guo, and J. Wei, Thermally driven photonic actuator based on silica opal photonic crystal with liquid crystal elastomer. *ACS Appl. Mater. Interfaces*, vol. 8, no. 14, pp. 9440−9445, 2016

[3] A. Guarino, G. Poberaj, D. Rezzonico, R. Degl'Innocenti, and P. Gunter, Electro-optically tunable microring resonators in lithium niobate, *Nat. Photonics*, vol. 1, no. 7, pp. 407−410, 2007.

[4] R. Takigawa, E. Higurashi, T. Suga, and T. Kawanishi, Air-gap structure between integrated $LiNbO_3$ optical modulators and micromachined Si substrates. *Opt. Express*, vol. 19, no. 17, pp. 15739-15749, 2011.

[5] Z. Zhu, P. G. Evans, R. F. Haglund Jr, and J. G. Valentine, Dynamically reconfigurable metadevice employing nanostructured phase-change materials, *Nano Lett.*, vol. 17, no. 8, pp.4881−4885, 2017.

[6] F. Raineri et al., Tuning a two-dimensional photonic crystal resonance via optical carrier injection, *Optics Lett.*, vol. 30, no. 1, pp.64-66, 2005.

[7] J. Rosenberg, Q. Lin, and O. Painter, Static and dynamic wavelength routing via the gradient optical force, *Nat. Photonics,* vol. 3, no. 8, pp. 478−483, 2009.

[8] G. S. Wiederhecker, L. Chen, A. Gondarenko, and M. Lipson, Controlling photonic structures using optical forces, *Nature*, vol. 462, no. 7273, pp. 633−636, 2009.

[9] A. Chatterjee, B. Bhuva, and R. Schrimpf, High-speed light modulation in avalanche breakdown mode for Si diodes. *IEEE Electron Device Lett.*, vol. 25, no. 9, pp. 628−630, 2004.

[10] K. Xu, Silicon MOS optoelectronic micro-nano structure based on reverse-biased PN junction. *Phys. Status Solidi (a)*, vol. 216, no. 7, pp.1800868, 2019.

[11] Q. Wang, D. Mao, and L. Dong, Thermomechanically tunable infrared metamaterials using asymmetric split-ring resonators, *J. Microelectromech. S.*, vol. 26, no. 6, pp. 1186−1188, 2017.

[12] Q. Wang et. al., NEMS-based infrared metamaterial via tuning nanocantilevers within complementary split ring resonators, *J. Microelectromech. S.*, vol. 26, no. 6, pp.1371−1380, 2017.

[13] W. Frank, P. B. Deotare, M. W. McCutcheon, and M. Loncar, Programmable photonic crystal nanobeam cavities, *Opt. Express*, vol.18, no. 8, pp. 8705−8712, 2010.

[14] T. Takahata, K. Matsumoto, and I. Shimoyama, A wide wavelength range optical switch using a flexible photonic crystal waveguide and silicon rods, *J. Micromech. Microeng.*, vol. 20, no. 7, p.075009, 2010.

[15] D. Mao, X. Qiao, and L. Dong, Design of nano-opto-mechanical reconfigurable photonic integrated circuit, *ýJ. Light. Technol*., vol. 31, no. 10, 1660−1669, 2013.

[16] D. Mao, P. Liu, K. M. Ho, and L. Dong, A theoretical study of a nano-opto-mechanical sensor using a photonic crystal-cantilever cavity, *J. Opt.,* vol. 14, p.075002, 2012.

[17] M. Notomi, E. Kuramochi, and H. Taniyama, Ultrahigh-Q nanocavity with 1D photonic gap, *Opt. Express*, vol. 16, no. 15, pp.11095−11102, 2008.

[18] Q. M. Quan and M. Loncar, Deterministic design of wavelength scale, ultra-high Q photonic crystal nanobeam cavities, *Opt. Express*, vol. 19, no. 19, pp. 18529-18542, 2011.

[19] F. Tian, G. Zhou, Y. Du, F. S. Chau, J. Deng, and R. Akkipeddi, Out-of-plane nanomechanical tuning of double-coupled one-dimensional photonic crystal cavities, *Opt. Lett.*, vol. 38, no. 12, pp. 2005-2007, 2013.

[20] T. Lin, X. Zhang, Y. Zou, F. S. Chau, J. Deng, and G. Zhou, Out-of-plane nano-electro-mechanical tuning of the Fano resonance in photonic crystal split-beam nanocavity, Appl. Phys. Lett., vol. 107, no. 15, p. 153107, 2015.